Available online at www.sciencedirect.com
SCIENCE DIRECT®
Journal of Sound and Vibration 266 (2003) 759–774
JOURNAL OF SOUND AND VIBRATION
www.elsevier.com/locate/jsvi

Dynamics modelling of a flexible hub–beam system with a tip mass

Hui Yang, Jiazhen Hong*, Zhengyue Yu

School of Civil Engineering and Mechanics, Shanghai Jiaotong University, Shanghai 200030, People's Republic of China

Received 1 October 2001; accepted 19 September 2002

Abstract

This paper presents a finite-element model for a flexible hub–beam system with a tip mass. Both viscous damping and air drag force are introduced into this model. The complete coupling between the system rigid and flexible degrees of freedom is allowed since the start of the formulation and developing the system kinematic variables. Based on deformation theory and geometric constraints, a second order approximation for the displacement field is proposed and the dynamic stiffening is accounted for. Hamilton's principle is utilized in deriving the equations of motion. The corresponding dynamics models of the tip mass and damping forces are developed in a consistent manner through formulating their energy expressions and applying Hamilton's principle. The finite element method is employed for spatial discretization due to its versatility, high accuracy and convergence. Numerical simulations show that the second order term in deformation field can have significant effect on dynamics behavior of flexible multibody systems. It is also shown that the traditional linear model cannot account for dynamic stiffening and may lead to erroneous result in some high-speed systems because the deformation field commonly used in structural dynamics is straight employed in this model. In contrast, the developed model (CCM) based on the second order deformation field can predict valid results. The effects of tip mass and damping on dynamics behavior of the hub–beam system are also discussed.

1. Introduction

Flexible multibody dynamics emerged as a new field in the early 1970s, and it had sparked the interest of many investigators in the mechanical engineering community, as well as in the control engineering area. Important applications of this research activity involve understanding and

*Corresponding author. Fax: +86-21-62933082.
E-mail address: jzhong@mail.sjtu.edu.cn (J. Hong).

0022-460X/03/$ - see front matter
doi:10.1016/S0022-460X(02)01332-9

control of the behaviors of flexible structures, such as light robotic manipulator, satellite solar array and space vehicles.

The hybrid co-ordinate approach [1–3] is currently the most widely used method for the dynamics simulation of complex flexible multibody systems. In this approach, the coupling between the rigid-body motion and the elastic deformations is taken into consideration and two sets of co-ordinates are employed to describe the configuration of the deformable bodies: one set describes the location and orientation of a selected body co-ordinate system, while the second set describes the deformation of the body with respect to its co-ordinate system. The deformation field commonly used in structural dynamics is straight adopted to determine the kinematics of flexible components in the system. Therefore, this approach does not account for modal characteristic changes due to reference rotational speeds of flexible components. As pointed out in Ref. [4], the traditional deformation field fails to produce an elastic rotation matrix that is complete to second order in the deformation variables.

The flexible hub–beam system is a typical multibody system and has been widely studied by numerous researchers. Kane et al. [5] investigated the beam undergoing large overall motions and reported that the conventional hybrid co-ordinate approach could lead to erroneous results such as prediction of dynamic softening of a rotating structure when dynamic stiffening is to be expected. Subsequently, many valuable researches on rotating beams had been done to modify the conventional hybrid co-ordinate approach in order to account for dynamic stiffening. Banerjee and Dickens [6] captured the dynamic stiffening terms and incorporated them into the system equations of motion by geometric constraints between transverse and longitudinal deflections in beams or plates. Liu and Liew [7], Wu and Haug [8] employ a system of substructures, where a flexible body is subdivided into many small sub-bodies (substructures or finite elements) with convected co-ordinate frames. Ider [9], Mayo and Dominguez [10] computed the dynamics stiffness matrix of a beam from the strain energy term including the non-linear strain–displacement relationship. Most of these investigations were concerned with the rotating beams or plates undergoing a prescribed large overall motion, wherein the effect of large overall motion of the reference frame on elastic deformation was considered but at the same time the beam's elastic deformation could not influence the large overall motion of the reference frame because the large over motion is known a priori. So the system reference frame equation of motion was not shown in the model with the associated effects from the system elastic deformations.

Chapnik et al. [11] reported a dynamic model for a rotating flexible arm impacted on its tip. They utilized the finite element method (FEM) in discretizing the beam reference motion and the beam elastic deformations. Yigit et al. [12] performed a study of the flexural motion of a radially rotating beam attached to a rotating base. The model is based on a generalized co-ordinate-shape function description. The study showed that for comparable inertia of the rigid shaft and of the flexible body, the uncoupled model might give incorrect results. But in this literature the effects of dynamic stiffening induced by the centrifugal force were not considered.

The present work is devoted towards establishing a finite-element model for a flexible hub–beam system, carrying a payload on its tip. Both viscous damping and air drag force are introduced into this model. The complete coupling between rigid and flexible degrees of freedom the system is allowed since the start of the formulation and developing the system kinematic variables. Based on deformation theory and geometric constraints, a second order approximation for the displacement field is proposed and the dynamic stiffening is accounted for. Hamilton's

principle is utilized in deriving the equation motion. The large overall motion of the beam reference frame is not prescribed and is certainly affected by elastic deformation since the motion of the hub is unknown a priori. The corresponding dynamics models of the tip mass and damping forces are developed in a consistent manner through formulating their energy expressions and applying Hamilton's principle. The FEM is employed for spatial discretization due to its versatility, high accuracy and convergence. Numerical simulations and comparisons with traditional hybrid co-ordinate approach are presented to demonstrate the validity of the developed model. The effects of tip mass and damping on dynamics behavior of the hub–beam system are also discussed.

2. Kinematics description

A schematic diagram of a flexible hub–beam system is shown in Fig. 1. The hub is assumed to be rigid and the flexible beam AB is attached radially to the hub at the point A. The beam has a slender shape so that shear and rotary inertia effects are neglected. The motion of the beam is confined to the horizontal plane and gravity is neglected and a tip mass is considered to be concentrated near the free end B of the beam. The rotary inertia of the tip mass is neglected. Two co-ordinate systems are necessary to describe the beam dynamics: an inertial frame $\mathbf{x}^0\mathbf{y}^0$ and a reference frame $\mathbf{xy}$ attached to the hub such that its $\mathbf{x}$-axis is directed along the undeformed configuration of the beam. The beam is described using n finite elements. Each finite element has its own co-ordinate system $\bar{x}\,\bar{y}$ attached to its first node i in its undeformed configuration. The position of the ith element co-ordinate system is defined by the position of the first node x_i in the $\mathbf{xy}$ reference frame.

To describe the motion of the beam in the inertia frame, introduce a differential element P_0Q_0 on the ith element. Point P_0 is located at a distance x along the undeformed centroidal axis from the origin of the reference frame. Let $\bar{x}$ denote the axial position of point P_0 measured relative to the $\bar{x}\,\bar{y}$ element co-ordinate system. Then the position vector of point P_0 with respect to the reference frame $\mathbf{xy}$ can be represented as

$$\boldsymbol{\rho}_P = (x \quad 0)^{\mathrm{T}} = (x_i + \bar{x} \quad 0)^{\mathrm{T}}. \tag{1}$$

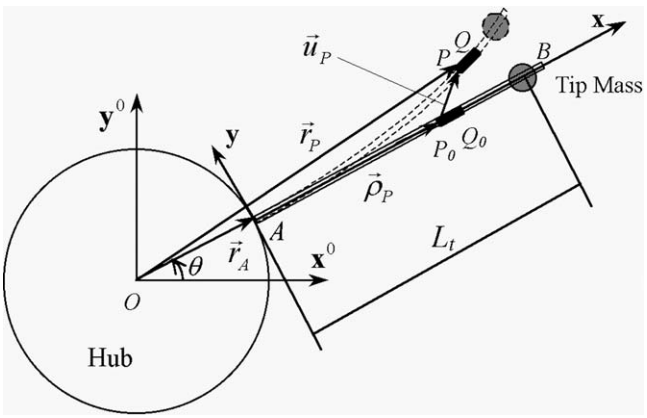

Fig. 1. Schematic diagram of a flexible hub–beam system.

After deformation, the differential element P_0Q_0 lies at a new position which is labelled PQ. The global position vector of point P can be written as

$$\mathbf{r}_P = \mathbf{r}_A + \mathbf{A}(\rho_P + \mathbf{u}_P), \tag{2}$$

where $\mathbf{r}_A$ is the position vector of the origin of the reference frame with respect to the inertia frame, $\mathbf{u}_P$ is the deformation vector and $\mathbf{A}$ is the rotational transformation matrix.

The velocity and acceleration vectors of point P can be obtained by differentiating Eq. (2) as follows:

$$\dot{\mathbf{r}}_P = \dot{\mathbf{r}}_A + \dot{\mathbf{A}}(\rho_P + \mathbf{u}_P) + \mathbf{A}\dot{\mathbf{u}}_P, \tag{3}$$

$$\ddot{\mathbf{r}}_P = \ddot{\mathbf{r}}_A - \dot{\theta}^2\mathbf{A}(\rho_P + \mathbf{u}_P) + 2\dot{\theta}\frac{\mathrm{d}\mathbf{A}}{\mathrm{d}\theta}\dot{\mathbf{u}}_P + \mathbf{A}\ddot{\mathbf{u}}_P + \ddot{\theta}\frac{\mathrm{d}\mathbf{A}}{\mathrm{d}\theta}(\rho_P + \mathbf{u}_P). \tag{4}$$

The deformation vector $\mathbf{u}_P$ can be written as

$$\mathbf{u}_P = (u_1 \quad u_2)^{\mathrm{T}}, \tag{5}$$

where u_1 and u_2 are the Cartesian distance measure of the beam deformation in the reference frame. After deformation, the arc-length of the differential element PQ is

$$\mathrm{d}s = \sqrt{\left(1 + \frac{\partial u_1}{\partial x}\right)^2 + \left(\frac{\partial u_2}{\partial x}\right)^2}\,\mathrm{d}x. \tag{6}$$

Using Taylor series expansion expression for radication, up to the second order terms of the deformation variables, $\mathrm{d}s$ can be written as

$$\mathrm{d}s = \left[1 + \frac{\partial u_1}{\partial x} + \frac{1}{2}\left(\frac{\partial u_2}{\partial x}\right)^2\right]\mathrm{d}x. \tag{7}$$

By integrating Eq. (7), the distance along the deformed elastic axis from point A to point P is

$$\widehat{AP} = \int_0^x \left[1 + \frac{\partial u_1}{\partial x} + \frac{1}{2}\left(\frac{\partial u_2}{\partial x}\right)^2\right]\mathrm{d}x. \tag{8}$$

Two variables are used to describe the deformation of point P: w_1, the pure axial deformation of the centroidal axis and w_2, the transverse deformation in the direction of the $\mathbf{y}$-axis of the reference frame. For a slender beam, the deformation w_2 is usually several orders of magnitude larger than the deformation w_1. So one can obtain $u_2 = w_2$. The arc-length $\widehat{AP}$ may also be expressed as

$$\widehat{AP} = x + w_1. \tag{9}$$

Using Eqs. (8) and (9), one obtains

$$u_1 = w_1 + w_c, \tag{10}$$

where w_c is a second order term

$$w_c = -\frac{1}{2}\int_0^x \left(\frac{\partial w_2}{\partial x}\right)^2 \mathrm{d}x. \tag{11}$$

It is clear from Eqs. (10) and (11) that the axial displacement of point P consists of two parts: the actual axial deformation of the point denoted as w_1 and the axial displacement of the point due to the inextensibility assumption, or the foreshortening effect, represented by w_c. It should be noted that the second order tem w_c is not included in the traditional linear deformation field but this term can have a significant impact on the beam's dynamic equations when it undergoes large rigid-body motion.

In view of slender beam and $x = x_i + \bar{x}$, substituting Eqs. (10) and (11) into Eq. (5) yields

$$\mathbf{u}_P = \begin{bmatrix} w_1 - \displaystyle\int_0^{x_i+\bar{x}} \frac{1}{2}\left(\frac{\partial w_2}{\partial x}\right)^2 \mathrm{d}x \\ w_2 \end{bmatrix}. \tag{12}$$

The FEM will be utilized to discretize the elastic beam. In the FEM, the deformations are usually represented in terms of the nodal degrees of freedom. This can be expressed as

$$w_1 = \mathbf{N}_1(\bar{x})\mathbf{q}(t), \quad w_2 = \mathbf{N}_2(\bar{x})\mathbf{q}(t), \tag{13}$$

where $\mathbf{N}_1(\bar{x})$ and $\mathbf{N}_2(\bar{x})$ are spatial-dependent matrices of the shape functions, and $\mathbf{q}(t)$ is the vector of nodal degrees of freedom which are time dependent.

Let l_i be the length of the ith element. Substituting Eq. (13) into Eq. (12) yields the deformation displacement vector of point P in the ith element

$$\mathbf{u}_P = \begin{bmatrix} \mathbf{N}_1\mathbf{q} - \frac{1}{2}\mathbf{q}^{\mathrm{T}}\mathbf{S}(i,\bar{x})\mathbf{q} \\ \mathbf{N}_2\mathbf{q} \end{bmatrix}, \tag{14}$$

where

$$\mathbf{S}(i,\bar{x}) = \int_0^{\bar{x}} \frac{\partial \mathbf{N}_2}{\partial \bar{x}}^{\mathrm{T}} \cdot \frac{\partial \mathbf{N}_2}{\partial \bar{x}} \mathrm{d}\bar{x} + \sum_{j=1}^{i-1} \int_0^{l_j} \frac{\partial \mathbf{N}_2}{\partial \bar{x}}^{\mathrm{T}} \cdot \frac{\partial \mathbf{N}_2}{\partial \bar{x}} \mathrm{d}\bar{x}. \tag{15}$$

It is easy to see that $\mathbf{S}(i,\bar{x})$ is a symmetrical and non-negative-definite matrix. The second order deformation field for a beam has been established as Eq. (15). In case of the second order term $\mathbf{S}(i,\bar{x})$ being neglected, Eq. (14) describes the traditional deformation field in the structural dynamics.

3. Dynamics equations

Let ρ denotes the mass per unit length for a typical element i, Then the system kinetic energy

$$T = T_H + T_L + \frac{1}{2}\sum_{i=1}^{n} \int_0^{l_i} \rho \dot{\mathbf{r}}_P^{\mathrm{T}} \dot{\mathbf{r}}_P \mathrm{d}x, \tag{16}$$

where T_H and T_L are the kinetic energy of the hub and of the tip mass, respectively.

By using Euler–Bernoulli theory, the potential energy is given by

$$\Pi = \frac{1}{2}\int_0^{l_i} EA_r\left(\frac{\partial w_1}{\partial x}\right)^2 \mathrm{d}x + \frac{1}{2}\int_0^{l_i} EI\left(\frac{\partial^2 w_2}{\partial x^2}\right)^2 \mathrm{d}x, \tag{17}$$

in which E is Young's modulus, A_r is the cross-sectional area and I is the area moment of inertia.

3.1. Equations of motion at the element level

To produce equations of motion in a compact form, the following element coefficients and matrices are introduced:

$$J_i = \int_0^{l_i} \rho(r_A + x_i + \bar{x})^2 \,\mathrm{d}\bar{x}, \tag{18}$$

$$\mathbf{M}_i = \int_0^{l_i} \rho(\mathbf{N}_1^{\mathrm{T}}\mathbf{N}_1 + \mathbf{N}_2^{\mathrm{T}}\mathbf{N}_2)\,\mathrm{d}\bar{x}, \tag{19}$$

$$\mathbf{K}_i = \int_0^{l_i} \left[EA_r\left(\frac{\partial \mathbf{N}_1}{\partial \bar{x}}\right)^{\mathrm{T}}\left(\frac{\partial \mathbf{N}_1}{\partial \bar{x}}\right) + EI\left(\frac{\partial^2 \mathbf{N}_2}{\partial \bar{x}^2}\right)^{\mathrm{T}}\left(\frac{\partial^2 \mathbf{N}_2}{\partial \bar{x}^2}\right)\right] \mathrm{d}\bar{x}, \tag{20}$$

$$\mathbf{U}_{0k} = \int_0^{l_i} \rho\mathbf{N}_k \,\mathrm{d}\bar{x}, \quad k = 1,2, \quad \mathbf{U}_{1k} = \int_0^{l_i} \rho(x_i + \bar{x})\mathbf{N}_k \,\mathrm{d}\bar{x}, \quad k = 1,2, \tag{21}$$

$$\mathbf{D}_0 = \int_0^{l_i} \rho\mathbf{S}(i,\bar{x})\,\mathrm{d}\bar{x}, \quad \mathbf{D}_1 = \int_0^{l_i} (x_i + \bar{x})\rho\mathbf{S}(i,\bar{x})\,\mathrm{d}\bar{x}, \tag{22}$$

$$\mathbf{R} = \int_0^{l_i} \rho\mathbf{N}_1^{\mathrm{T}}\mathbf{N}_2 \,\mathrm{d}\bar{x}, \quad \mathbf{G}_i = \mathbf{R}^{\mathrm{T}} - \mathbf{R}, \tag{23}$$

where J_i is the moment of inertia of ith element about the hub center, the matrix $\mathbf{M}_i$ is the consistent mass matrix that usually appears in the structural dynamics finite element formulations and $\mathbf{K}_i$ is the conventional stiffness matrix. The matrices $\mathbf{R}$ and $\mathbf{G}_i$ result from the gyroscopic effects, while the matrices $\mathbf{D}_0$ and $\mathbf{D}_1$ result from the second order term of the deformation field. Both matrices $\mathbf{D}_0$ and $\mathbf{D}_1$ are non-negative definite because $\mathbf{S}(i,\bar{x})$ is a non-negative definite matrix.

By applying Hamilton's principle to Eqs. (16) and (17), the equations of motion at the element level can be written in compact form as

$$\begin{bmatrix} M_{\theta\theta} & \mathbf{M}_{\theta q} \\ \mathbf{M}_{q\theta} & \mathbf{M}_{qq} \end{bmatrix}\begin{bmatrix} \ddot{\theta} \\ \ddot{\mathbf{q}} \end{bmatrix} + 2\dot{\theta}\begin{bmatrix} 0 & 0 \\ 0 & \mathbf{G}_i \end{bmatrix}\begin{bmatrix} \dot{\theta} \\ \dot{\mathbf{q}} \end{bmatrix} + \mathbf{C}\begin{bmatrix} \dot{\theta} \\ \dot{\mathbf{q}} \end{bmatrix} + \begin{bmatrix} 0 & 0 \\ 0 & \mathbf{K}_{qq} \end{bmatrix}\begin{bmatrix} \theta \\ \mathbf{q} \end{bmatrix} = \begin{bmatrix} Q_\theta \\ \mathbf{Q}_q \end{bmatrix} + \begin{bmatrix} F_\theta \\ \mathbf{F}_q \end{bmatrix}, \tag{24}$$

where

$$M_{\theta\theta} = J_i + \mathbf{q}^{\mathrm{T}}\mathbf{M}_i\mathbf{q} + 2(r_A\mathbf{U}_{01} + \mathbf{U}_{11})\mathbf{q} - \underline{\mathbf{q}^{\mathrm{T}}(r_A\mathbf{D}_0 + \mathbf{D}_1)\mathbf{q}}, \tag{25}$$

$$\mathbf{M}_{\theta q} = \mathbf{M}_{q\theta}^{\mathrm{T}} = r_A\mathbf{U}_{02} + \mathbf{U}_{12} + \mathbf{q}^{\mathrm{T}}\mathbf{G}_i, \quad \mathbf{M}_{qq} = \mathbf{M}_i, \tag{26}$$

$$\mathbf{K}_{qq} = \mathbf{K}_i - \dot{\theta}^2\mathbf{M}_i + \underline{\dot{\theta}^2(r_A\mathbf{D}_0 + \mathbf{D}_1)}, \tag{27}$$

$$Q_\theta = -2\dot{\theta}\left[\mathbf{q}^{\mathrm{T}}\mathbf{M}_i\dot{\mathbf{q}} + (r_A\mathbf{U}_{01} + \mathbf{U}_{11})\dot{\mathbf{q}} - \underline{\mathbf{q}^{\mathrm{T}}(r_A\mathbf{D}_0 + \mathbf{D}_1)\dot{\mathbf{q}}}\right], \tag{28}$$

$$\mathbf{Q}_q = \dot{\theta}^2(r_A\mathbf{U}_{01}^{\mathrm{T}} + \mathbf{U}_{11}^{\mathrm{T}}). \tag{29}$$

In addition, F_θ represents the rotational external torque and the matrix $\mathbf{F}_q$ is the vector of nodal external forces. The matrix $\mathbf{C}$ is damping matrix that will be discussed later. The underlined terms in Eqs. (25), (27) and (28) are the terms resulting from the second order deformation field.

In Eq. (24), one can recognize the non-linear inertia coupling between the rigid-body motion and the elastic deformations. The entry $\mathbf{M}_{\theta\theta}$ is the rotational inertia of the system, and $\mathbf{M}_{qq}$ is the beam generalized elastic mass matrix. The entry $\mathbf{M}_{\theta q}$ represents the non-linear inertia coupling between the motion of the reference frame and the elastic deformations. The matrix $\mathbf{K}_{qq}$ is the generalized elastic stiffness matrix that is shown to be affected by both the motion of the reference frame and the elastic deformations. The effects can be visualized to be both stiffening and softening.

3.2. Tip mass dynamics

The tip mass, as shown in Fig. 1, is located at a distance L_t along the undeformed centroidal axis from the origin of the reference frame **xy**. It is considered to have a mass m_t and attached to the nth element. The position of the nth element co-ordinate system in the **xy** reference frame is x_n, and $\gamma = L_t - x_n$ is the axial position of the tip mass measured relative to the nth element co-ordinate system in the undeformed configuration. Then the position vector of the tip mass with respect to the inertial frame $\mathbf{x}^0\mathbf{y}^0$ can be represented as

$$\mathbf{r}_L = \mathbf{r}_A + \mathbf{A}(\boldsymbol{\rho}_L + \mathbf{u}_L), \tag{30}$$

where $\boldsymbol{\rho}_L = (L_t \ 0)^{\mathrm{T}}$ is the position vector of the tip mass in the reference frame **xy** in the undeformed configuration, and $\mathbf{u}_L$ is the elastic displacement vector of the tip mass.

The acceleration vector of the tip mass is obtained by differentiating Eq. (30) two times and found to be in the form

$$\ddot{\mathbf{r}}_L = \ddot{\mathbf{r}}_A - \dot{\theta}^2\mathbf{A}(\rho_L + \mathbf{u}_L) + 2\dot{\theta}\frac{\mathrm{d}\mathbf{A}}{\mathrm{d}\theta}\dot{\mathbf{u}}_L + \mathbf{A}\ddot{\mathbf{u}}_L + \ddot{\theta}\frac{\mathrm{d}\mathbf{A}}{\mathrm{d}\theta}(\rho_L + \mathbf{u}_L). \tag{31}$$

The tip mass contributes to the dynamics of the system through its kinetic energy, and only the translational kinetic energy of the tip mass is taken into account because the rotary inertia of the tip mass is neglected. The variation of the translational kinetic energy of the tip mass can be expressed as

$$\delta T_L = -m_t\delta\mathbf{r}_L^{\mathrm{T}}\ddot{\mathbf{r}}_L. \tag{32}$$

The contribution of the tip mass to the dynamics of the system can also be included by applying Hamilton's principle to Eq. (32). After differentiation and algebraic manipulations, the equations

can be represented by the following matrix form:

$$\begin{bmatrix} M_{\theta\theta}^L & \mathbf{M}_{\theta q}^L \\ \mathbf{M}_{q\theta}^L & \mathbf{M}_{qq}^L \end{bmatrix} \begin{bmatrix} \ddot{\theta} \\ \ddot{\mathbf{q}} \end{bmatrix} + 2\dot{\theta} \begin{bmatrix} 0 & 0 \\ 0 & \mathbf{G}^L \end{bmatrix} \begin{bmatrix} \dot{\theta} \\ \dot{\mathbf{q}} \end{bmatrix} + \begin{bmatrix} 0 & 0 \\ 0 & \mathbf{K}_{qq}^L \end{bmatrix} \begin{bmatrix} \theta \\ \mathbf{q} \end{bmatrix} = \begin{bmatrix} Q_\theta^L \\ \mathbf{Q}_q^L \end{bmatrix}, \tag{33}$$

where the coefficients and matrices are shown in the appendix.

3.3. Equation of the hub

The contribution of the hub to the dynamics of the system can be represented as

$$\begin{bmatrix} J_H & 0 \\ 0 & 0 \end{bmatrix} \begin{bmatrix} \ddot{\theta} \\ \ddot{\mathbf{q}} \end{bmatrix} = \begin{bmatrix} 0 \\ 0 \end{bmatrix}, \tag{34}$$

where J_H is the rotary inertia of the hub.

3.4. Damping

It is realized that the presence or absence of damping has a dramatic effect on dynamics of some modern flexible structures, particularly for large initial displacements with high velocities. So the effects of atmosphere and viscous structural damping are taken into account in the present model of hub–beam system, and this model may be useful for future experiment. We consider three kinds of damping: Rayleigh beam damping, viscous hub friction and air drag forces.

Rayleigh's proportional damping in the beam material has been assumed. The structural damping matrix of element i can be expressed as

$$\mathbf{C}_S = b_1\mathbf{M}_i + b_2\mathbf{K}_i, \tag{35}$$

where b_1 and b_2 are mass damping coefficient and stiffness damping coefficient, respectively. The matrix $\mathbf{M}_i$ is the consistent mass matrix and $\mathbf{K}_i$ is the conventional stiffness matrix, as shown in Eqs. (19) and (20).

When a thin plate rotates and vibrates transversely in air, the air drag force can cause free vibrations to decay. As reported in Refs. [13,14], one must consider two types of drag forces, namely one proportional to the instantaneous velocity and the other proportional to the square of the instantaneous velocity. Based on these reports, the air drag forces per unit length on the beam slewing about the hub center axis can be written as

$$\mathbf{F}_{A1} = -\beta_1\dot{\mathbf{r}}_P \tag{36}$$

and

$$\mathbf{F}_{A2} = -\beta_2\dot{\mathbf{r}}_P|\dot{\mathbf{r}}_P|, \tag{37}$$

where β_1 and β_2 are two coefficients.

By using Eqs. (3) and (36), the virtual work produced by the linear drag force $\mathbf{F}_{A1}$ acting on ith element has the form

$$\delta W_{A1} = -\beta_1 \int_0^{l_i} \delta\mathbf{r}_P^{\mathrm{T}} [\dot{\mathbf{r}}_A + \dot{\mathbf{A}}(\rho_P + \mathbf{u}_P) + \mathbf{A}\dot{\mathbf{u}}_P] \,\mathrm{d}\bar{x}. \tag{38}$$

By utilizing Hamilton's principle, the contribution of the drag force proportional to the velocity to the dynamics of the system can be represented by the following damping matrix:

$$\mathbf{C}_{A1} = -\frac{\beta_1}{\rho}\begin{bmatrix} M_{\theta\theta} & \mathbf{M}_{\theta q} \\ \mathbf{M}_{q\theta} & \mathbf{M}_{qq} \end{bmatrix}. \tag{39}$$

It is clear that this damping matrix due to the drag force proportional to the velocity has the same expression as the generalized mass matrix in Eq. (24) except different coefficients.

By substituting Eq. (3) into Eq. (37), the drag force proportional to the velocity squared can be rewritten as

$$\mathbf{F}_{A2} = -\beta_2[\dot{\mathbf{r}}_A + \dot{\mathbf{A}}(\rho_P + \mathbf{u}_P) + \mathbf{A}\dot{\mathbf{u}}_P]\left|\dot{\mathbf{r}}_A + \dot{\mathbf{A}}\rho_P + \dot{\mathbf{A}}\mathbf{u}_P + \mathbf{A}\dot{\mathbf{u}}_P\right|. \tag{40}$$

The expression of this drag force is very complicated, and it would lead to non-linear equations of motion that are difficult to solve analytically and even numerically; thus some simplification is helpful. For the case of a fast slew maneuver of the flexible beam, the instantaneous velocity $\dot{\mathbf{r}}_A + \dot{\mathbf{A}}\rho_P$ due to the hub angular velocity is usually one order of magnitude higher than the instantaneous velocity $\dot{\mathbf{A}}\mathbf{u}_P + \mathbf{A}\dot{\mathbf{u}}_P$ due to the elastic deformation [14]. Therefore, Eq. (40) can be reduced to

$$\mathbf{F}_{A2} = -\beta_2[\dot{\mathbf{r}}_A + \dot{\mathbf{A}}(\rho_P + \mathbf{u}_P) + \mathbf{A}\dot{\mathbf{u}}_P]\left|\dot{\mathbf{r}}_A + \dot{\mathbf{A}}\rho_P\right|. \tag{41}$$

Similar to deriving the matrix $\boldsymbol{C}_{A1}$, the contribution of the drag force $\boldsymbol{F}_{A2}$ to the dynamics of the system can also be represented by a damping matrix

$$\mathbf{C}_{A2} = -\frac{\beta_2\dot{\theta}\,\mathrm{sign}\,(\dot{\theta})}{\rho}\begin{bmatrix} C_{b1} & \mathbf{C}_{b2} \\ \mathbf{C}_{b3} & \mathbf{C}_{b4} \end{bmatrix}, \tag{42}$$

where

$$C_{b1} = \int_0^{l_i} \rho(r_A + x_i + \bar{x})^3\,\mathrm{d}\bar{x}, \tag{43}$$

$$\mathbf{C}_{b2} = 2r_A\mathbf{U}_{12} + r_A^2\mathbf{U}_{02} + \int_0^{l_i} \rho(x_i + \bar{x})^2\mathbf{N}_2\,\mathrm{d}\bar{x}, \tag{44}$$

$$\mathbf{C}_{b3} = \mathbf{C}_{b2}^{\mathrm{T}}, \quad \mathbf{C}_{b4} = r_A\mathbf{M}_i + \int_0^{l_i} \rho(x_i + \bar{x})\mathbf{N}_2^{\mathrm{T}}\mathbf{N}_2\,\mathrm{d}\bar{x}. \tag{45}$$

After including the effect of viscous hub friction, the global damping matrix has the form

$$\mathbf{C} = \begin{bmatrix} C_H & 0 \\ 0 & b_1\mathbf{M}_i + b_2\mathbf{K}_i \end{bmatrix} + \frac{\beta_1}{\rho}\begin{bmatrix} M_{\theta\theta} & \mathbf{M}_{\theta q} \\ \mathbf{M}_{q\theta} & \mathbf{M}_{qq} \end{bmatrix} + \frac{\beta_2\dot{\theta}\,\mathrm{sign}\,(\dot{\theta})}{\rho}\begin{bmatrix} C_{b1} & \mathbf{C}_{b2} \\ \mathbf{C}_{b3} & \mathbf{C}_{b4} \end{bmatrix}, \tag{46}$$

where C_H is viscous friction coefficient. Substituting Eq. (46) into Eq. (24) yields the equations of motion including the effects of damping at the element level.

3.5. Equations of motion of the whole system

Now, the global equations of motion of the hub–beam system with tip mass can be established by the conventional finite element assembling procedure of the elemental coefficient matrices. The entries of Eqs. (33) and (34) are to be added to the corresponding entries of the generalized matrices in the equation of motion of the whole system.

Two different dynamics models are developed in order to examine the effect of the proposed second order deformation field on the response of the hub–beam system. In the first model, called *consistent complete model* (CCM), the effect of second order deformation field is included. The CCM is just the proposed model above. In the second model, called *traditional linear model* (TLM), the effect of second order deformation field is neglected, so one has $\mathbf{S}(i,\bar{x})=0$ and $\mathbf{D}_0=\mathbf{D}_1=0$ in Eq. (22).

Both models are based FEM, since FEM has some advantages compared to the mode method. It is known that large overall motion can affect the vibration modal frequencies and shape functions of the beam. Therefore, the modal characteristics of the rotating beam are some different from that of the non-rotating beam. At the same time, selection of deformation mode is important for the accuracy of the solution. In general, more than three modes are used to discretize the governing equations in order to maintain enough accuracy of numerical results. If FEM is adopted to build the equation of motion, there is no need to select modal shape functions because the beam has been divided into some small elements and interpolation function is used to discretize the beam element. In addition, very accurate solutions are obtained with a well-known guarantee of convergence [15].

4. Numerical simulation

4.1. Maneuver of a hub–beam system

Consider first a hub–beam system, as shown in Fig. 1. A prescribed torque $\tau(t)$ pulse applied to the hub was chosen as an input to the system, and it has the following profile:

$$\tau(t)=\begin{cases}\tau_P, & 0\leqslant t\leqslant t_1,\\ 0, & t_2\leqslant t\leqslant t_3,\\ t_1, & -\tau_P.\end{cases} \tag{47}$$

The tip mass is assumed to be zero and the effects of damping are neglected. The objective is to determine the time history response of the system. (This model was studied by Yigit et al. [12].) The values of parameters involved are the same as in Ref. [12] and are as follows: beam length $L=0.5\,\mathrm{m}$, $\rho=0.0858\,\mathrm{kg/m}$, $EI=5.50\,\mathrm{N\,m^2}$, $J_H=7.845\times10^{-4}\,\mathrm{kg\,m^2}$, $m_t=0$, $r_A=0.05\,\mathrm{m}$, $\tau_P=1.0\,\mathrm{N\,m}$, $t_1=0.05\,\mathrm{s}$, $t_2=0.1\,\mathrm{s}$, $t_3=0.15\,\mathrm{s}$.

Figs. 2 and 3 show the results of the simulations using the two models (CCM, TLM) discussed in the preceding sections. It is clear that no substantial differences are found between the result (tip deflection of the beam or angular velocity of the hub) of the CCM and TLM, and the results of CCM (and TLM) agree with those presented in Ref. [12]. It should be noted that Yigit et al. [12] obtained the results by using assumed mode method (Galerkin method) and they found that using only a one mode approximation can also produce perfect solutions for the case $m_t=0$.

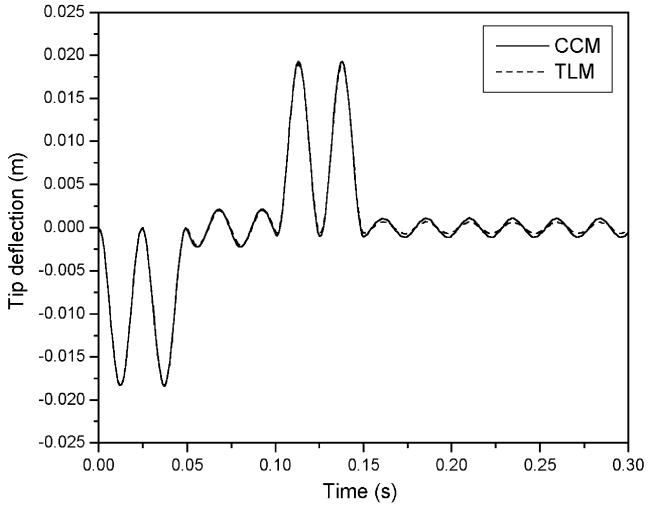

Fig. 2. Beam tip deflection ($m_t = 0$).

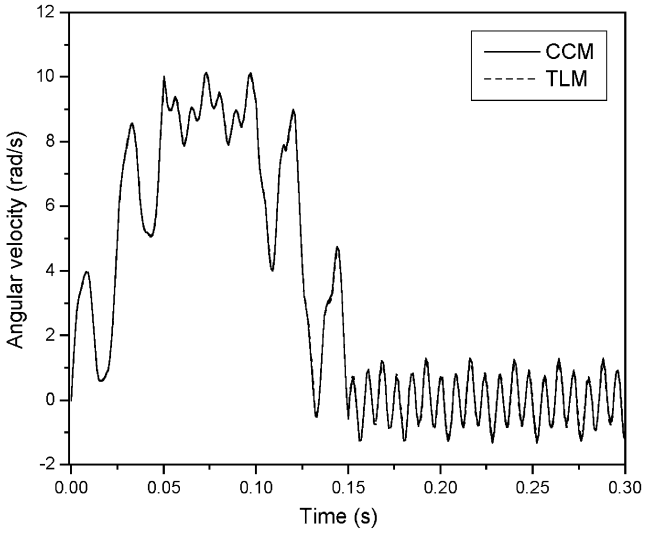

Fig. 3. Angular velocity of the hub ($m_t = 0$).

With same parameters as above except $m_t = 0.015\,\text{kg}$, the simulations are performed again. Fig. 4 shows the beam tip deflection obtained by using the CCM. When compared to the case without tip mass in Fig. 2, it can be seen that the tip mass has the effect of decreasing the frequency of oscillations, and increasing the amplitude in the period of the first pulse (0–0.5 s). Fig. 5 shows the resulting tip deflection obtained by using assumed mode method. Here, admissible functions are chosen as the mode shapes for the non-rotating cantilever beam with a tip mass. If compared to Fig. 4, it is clear that using only a one mode approximation leads to an erroneous result: the first order vibration frequency of the beam is much higher than that obtained by FEM. If the first three modes from a clamped-mass boundary condition are used for numerical simulation, the resulting frequency is coincident with the frequency obtained by FEM. For more

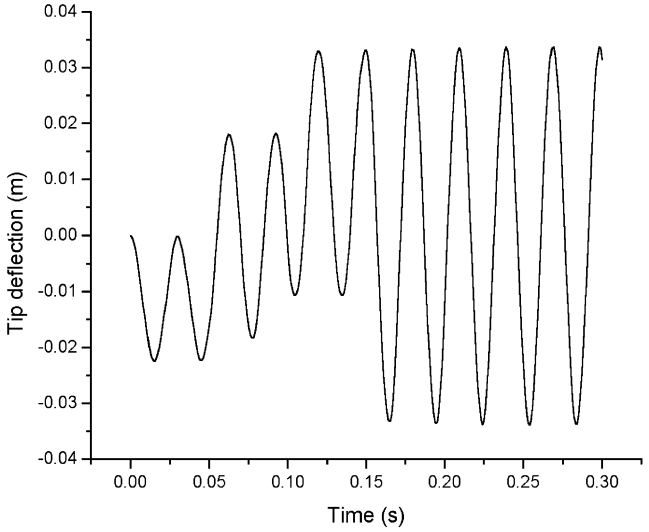

Fig. 4. Beam tip deflection obtained by FEM ($m_t = 0.015\,\text{kg}$).

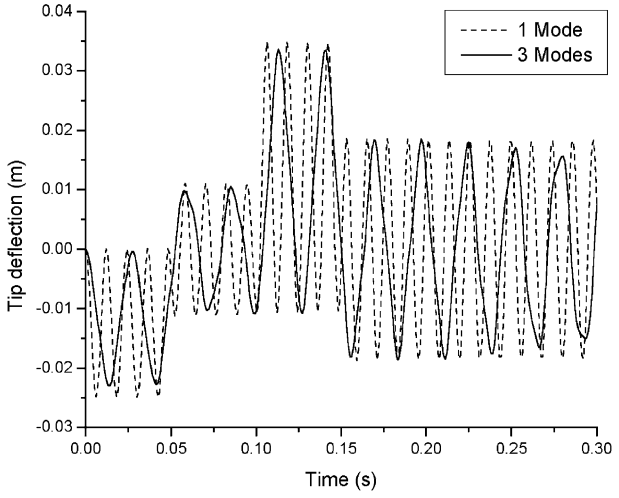

Fig. 5. Beam tip deflection obtained by assumed mode method ($m_t = 0.015\,\text{kg}$).

accurate results, more than three modes must be used, or one can chose other complex global or system modes, which is seriously dependent on personal experience.

For this example, accurate results can be predicted with the traditional linear deformation field (CCM and TLM). This is not always the case, as will be demonstrated in the second example.

4.2. Free vibration of a hub–beam system

In this example, both the tip mass and the damping are taken into account, but neither external force nor torque was applied to the hub–beam system as shown in Fig. 1. A uniform beam made

Table 1
Summary of model parameters

Property	Symbol	Value
Beam length	L	1.80 m
Mass per unit length	ρ	0.69167 kg/m
Cross-section	A_r	$0.00025\,m^2$
Young's modulus	E	$6.8952 \times 10^{10}\,N/m^2$
Beam area moment of inertia	I	$1.3021 \times 10^{-10}\,m^4$
Hub moment of inertia	J_H	$1.16\,kg\,m^2$
Tip mass	m_t	0.09 kg
Hub radius (distance from point O to point A)	r_A	0.121 m
Mass damping coefficient	b_1	0.056
Stiffness damping coefficient	b_2	0
Coefficient of air drag force	β_1	0.3
Coefficient of air drag force	β_2	0
Viscous friction coefficient	C_H	0

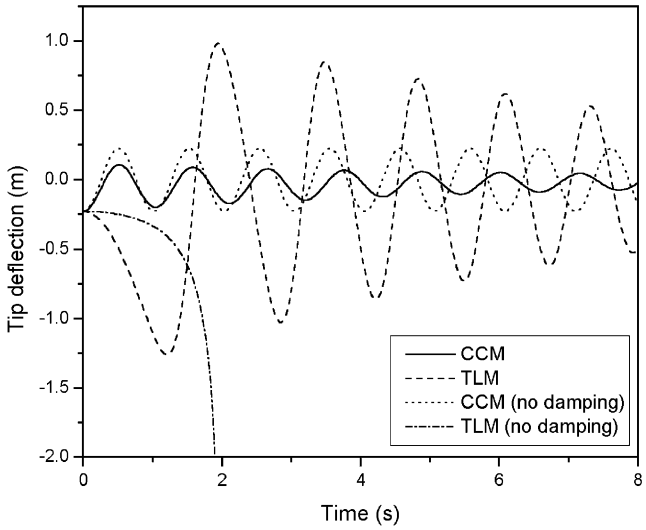

Fig. 6. Beam tip deflection.

of aluminum with the dimensions and material properties given in Table 1 is used in the present numerical simulation. The fundamental frequency of this beam for clamped–free condition is 0.548 Hz. A tip mass m_t is concentrated in the free end of the beam.

The beam is given an initial tip deflection of 0.229 m. The angular position of the hub is set to zero at $t = 0$, and the angular velocity of the hub is initially given by 3.473 rad/s. The time histories of the resulting tip deflection of the beam by using the two models (CCM, TLM) are shown in Fig. 6. The results of the beam tip deflection when all effects of damping are neglected are also shown in Fig. 6. It can be seen that the important difference has occurred between the beam tip deflection by using the CCM (solid line) and that by using the TLM (dashed line). Due to

the effects of damping the tip deflection of the beam using the CCM has a trend of decaying since the start of simulation, and the maximal tip deflection is the initial tip deflection 0.229 m. To gain more information about the resulting dynamics behavior of the system, the FFT spectrum analysis is employed. It is found that the waveform of the beam tip deflection using the CCM is dominated by a fundamental mode (0.879 Hz) with a small third mode component (10.16 Hz) superimposed on it. This fundamental frequency (0.879 Hz) is 60% higher than the fundamental frequency for clamped–free condition (0.548 Hz), and this phenomenon of frequency increase can also be seen in Ref. [12]. Compared to the resulting tip deflection using the CCM, the TLM shows a substantially different behavior: at first the beam tip deflection in the TLM increases to a large deflection about 1.26 m, and then tends to oscillate with decaying. It is noteworthy to mention that the amplitude of the resulting tip deflection using the TLM is much larger than that using the CCM, and even the resulting tip deflection using the TLM has exceeded the assumption of small deformation. At the same time, the TLM has lower fundamental frequency (0.730 Hz) than the CCM (0.879 Hz).

The dot line and dash–dot line in Fig. 6 represent the tip deflections of the beam obtained using (the two models) CCM and TLM without damping, respectively. When the effects of damping are neglected, the CCM has a higher fundamental frequency (0.988 Hz). But the tip deflection of the beam obtained using the TLM without damping indicates a cataclysmic instability of the motion. Physically, it seems clear that this system does not have instabilities and so it is the modelling (TLM) that is incorrect. This can be explained from the stiffness matrix in Eq. (27). Because the second order term in deformation field is not included, the generalized elastic stiffness matrix in the TLM is expressed as $\mathbf{K}_{qq} = \mathbf{K}_i - \dot{\theta}^2\mathbf{M}_i$. From this expression, it is recognized that the increase of the hub angular velocity $\dot{\theta}$ could cause a "softening" effect on the elastic stiffness matrix $\mathbf{K}_{qq}$. If the angular velocity of the hub is higher than a critical value (i.e., the fundamental frequency of the beam), this elastic stiffness matrix may be negative definite and the system becomes unstable. On the other hand, the generalized elastic stiffness matrix in the CCM is represented as $\mathbf{K}_{qq} = \mathbf{K}_i - \dot{\theta}^2\mathbf{M}_i + \dot{\theta}^2(r_A\mathbf{D}_0 + \mathbf{D}_1)$, in which the inclusion of the non-negative definite matrix $\dot{\theta}^2(r_A\mathbf{D}_0 + \mathbf{D}_1)$ can fully counteract the effect of softening mentioned above. (It is well known that high-speed rotating can cause the so-called "dynamic stiffening" instead of "softening".) So the CCM leads to a well-behaved response as expected. For the TLM, the angular velocity $\dot{\theta}$ of the hub decreases due to the air damping and the effect of softening by $-\dot{\theta}^2\mathbf{M}_i$ becomes more and more weak. Hence the system stiffness rebounds gradually. Eventually, the responses of the TLM tend to oscillate with decaying, as shown in Fig. 6 (response of the beam tip deflection) and Fig. 7 (response of the hub angular velocity). However, the system stiffness of the TLM is still "softer" than that of the CCM. So the responses of the TLM show a lower-frequency but larger-amplitude characteristic. Although these results from the TLM with damping are numerically stable, they are still incorrect. From the above, it is seen that the second order term in deformation field can have significant effect on dynamics behavior of flexible multibody systems in high-speed case, and the developed model (CCM) based on the second order deformation field can predict valid results.

5. Conclusions

In this paper, a finite-element model for a flexible hub–beam system carrying a tip mass is presented. Both viscous damping and air drag force are introduced into this model. Based on

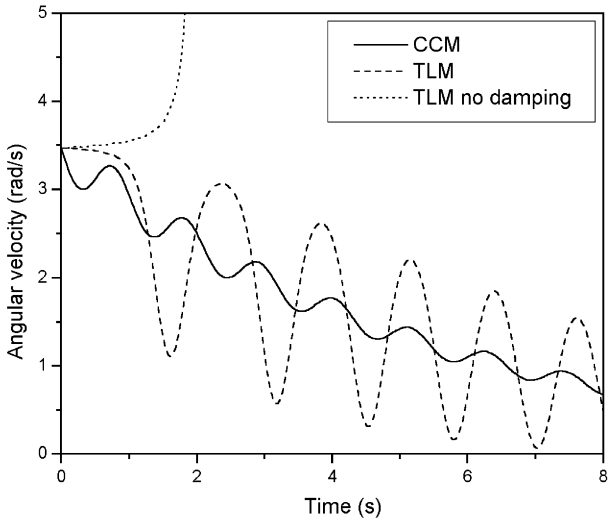

Fig. 7. Angular velocity of the hub.

deformation theory and geometric constraints, a second order approximation for the displacement field is proposed and the dynamic stiffening is accounted for. Since the motion of the hub is unknown a priori, the large overall motion of the reference frame of the beam is not prescribed but is influenced by elastic vibration. The corresponding dynamic models of the tip mass and damping forces are developed in a consistent manner through formulating the their energy expressions and applying Hamilton's principle. The FEM is used for spatial discretization due to its versatility, high accuracy and convergence. Numerical simulations and comparisons with traditional hybrid co-ordinate approach are presented to demonstrate the validity of the developed model. It is shown that the traditional hybrid co-ordinate approach cannot account for dynamic stiffening and may lead to erroneous result in some high-speed systems because of the softening effect on the elastic stiffness matrix. It is also seen that the damping can weaken this effect of softening. In future research, experimental investigations on such a system are needed.

Acknowledgements

The research is supported by the National Natural Science Foundation of China under Grant 19832040. This support is sincerely appreciated.

Appendix

The coefficients and matrices in the motion equation (33) of the tip mass are given as follows:

$$M_{\theta\theta}^{L} = m_t[(r_A + L_t)^2 + \mathbf{q}^{\mathrm{T}}\mathbf{N}_1^{\mathrm{T}}(\gamma)\mathbf{N}_1(\gamma)\mathbf{q} + \mathbf{q}^{\mathrm{T}}\mathbf{N}_2^{\mathrm{T}}(\gamma)\mathbf{N}_2(\gamma)\mathbf{q} + 2(r_A + L_t)\mathbf{N}_1(\gamma)\mathbf{q} - (r_A + L_t)\mathbf{q}^{\mathrm{T}}\mathbf{S}(n,\gamma)\mathbf{q}], \tag{A.1}$$

$$\mathbf{M}_{\theta q}^{L} = (\mathbf{M}_{q\theta}^{L})^{\mathrm{T}} = m_t[(r_A + L_t)\mathbf{N}_2(\gamma) + \mathbf{q}^{\mathrm{T}}\mathbf{N}_1^{\mathrm{T}}(\gamma)\mathbf{N}_2(\gamma) - \mathbf{q}^{\mathrm{T}}\mathbf{N}_2^{\mathrm{T}}(\gamma)\mathbf{N}_1(\gamma)], \tag{A.2}$$

$$\mathbf{M}_{qq}^{L} = m_t[\mathbf{N}_1^{\mathrm{T}}(\gamma)\mathbf{N}_1(\gamma) + \mathbf{N}_2^{\mathrm{T}}(\gamma)\mathbf{N}_2(\gamma)], \tag{A.3}$$

$$\mathbf{K}_{qq}^{L} = -m_t\dot{\theta}^2[\mathbf{N}_1^{\mathrm{T}}(\gamma)\mathbf{N}_1(\gamma) + \mathbf{N}_2^{\mathrm{T}}(\gamma)\mathbf{N}_2(\gamma)] + m_t\dot{\theta}^2(r_A + L_t)\mathbf{S}(n,\gamma), \tag{A.4}$$

$$\mathbf{G}^{L} = m_t[\mathbf{N}_2^{\mathrm{T}}(\gamma)\mathbf{N}_1(\gamma) - \mathbf{N}_1^{\mathrm{T}}(\gamma)\mathbf{N}_2(\gamma)], \tag{A.5}$$

$$\begin{aligned} Q_{\theta}^{L} = & -2m_t\dot{\theta}\{\mathbf{q}^{\mathrm{T}}\mathbf{N}_1^{\mathrm{T}}(\gamma)\mathbf{N}_1(\gamma)\dot{\mathbf{q}} + \mathbf{q}^{\mathrm{T}}\mathbf{N}_2^{\mathrm{T}}(\gamma)\mathbf{N}_2(\gamma)\dot{\mathbf{q}} \\ & + (r_A + L_t)[\mathbf{N}_1(\gamma)\dot{\mathbf{q}} - \mathbf{q}^{\mathrm{T}}\mathbf{S}(n,\gamma)\dot{\mathbf{q}}]\}, \end{aligned} \tag{A.6}$$

$$\mathbf{Q}_{q}^{L} = m_t\dot{\theta}^2(r_A + L_t)N_1^{\mathrm{T}}(\gamma). \tag{A.7}$$

References

[1] L. Meirovitch, D.A. Nelson, On the high-speed motion of satellite containing elastic parts, American Institute of Aeronautics and Astronautics, Journal of Spacecraft and Rockets 3 (11) (1966) 1597–1602.

[2] P.W. Likins, Finite element appendage equations for hybrid coordinate dynamic analysis, Journal of Solids and Structures 8 (1972) 709–731.

[3] L. Meirovitch, Hybrid state equations of motion for flexible bodies in terms of quasicoordinates, Journal of Guidance, Control and Dynamics 14 (5) (1990) 1374–1383.

[4] P. Shi, J. Mcphee, G.R. Heppler, A deformation field for Euler–Bernoulli beams with applications to flexible multibody dynamics, Multibody System Dynamics 5 (2001) 79–104.

[5] T.R. Kane, R.R. Ryan, A.K. Banerjee, Dynamics of a cantilever beam attached to a moving base, Journal of Guidance, Control and Dynamics 10 (2) (1987) 139–151.

[6] A.K. Banerjee, J.M. Dickens, Dynamics of an arbitrary flexible body in large rotation and translation, Journal of Guidance, Control and Dynamics 13 (2) (1990) 221–227.

[7] A.Q. Liu, K.M. Liew, Non-linear substructures approach for dynamic analysis of rigid-flexible multibody system, Computer Methods in Applied Mechanics and Engineering 114 (1994) 379–396.

[8] S.C. Wu, E.J. Haug, Geometric non-linear substructuring for dynamics of flexible mechanical system, International Journal for Numerical Methods in Engineering 26 (1988) 2211–2226.

[9] S.K. Ider, Finite element based recursive formulation for real time dynamic simulation of flexible multibody systems, Computers and Structures 40 (1991) 939–945.

[10] J. Mayo, J. Dominguez, Geometrically nonlinear formulation of flexible multibody systems in terms of beam elements: geometric stiffness, Computers and Structures 59 (1996) 1039–1050.

[11] B.V. Chapnik, G.R. Heppler, J.D. Aplevich, Modeling impact on a one-link flexible robotic arm, IEEE Transactions on Robotics and Automation 7 (4) (1991) 479–488.

[12] A. Yigit, R.A. Scott, A.G. Ulsoy, Flexural motion of a radially rotating beam attached to a rigid body, Journal of Sound and Vibration 121 (2) (1988) 201–210.

[13] W.E. Baker, E. Woolam, D. Young, Air and internal damping of thin cantilever beams, International Journal of Mechanical Sciences 9 (1967) 743–766.

[14] J.N. Juang, L.G. Horta, Effects of atmosphere on slewing control of a flexible structure, Journal of Guidance, Control and Dynamics 10 (4) (1987) 387–392.

[15] R.E. Valembois, P. Fisette, J.C. Samin, Comparison of various techniques for modelling flexible beams in multibody dynamics, Nonlinear Dynamics 12 (1997) 367–397.